Transcriptome Analysis of the Transdifferentiation of canine BMSCs into Insulin Producing Cells

JINGLU WANG
Northwest Agriculture and Forestry University
Pengxiu Dai
Northwest Agriculture and Forestry University
Tong Zou
Northwest Agriculture and Forestry University
Yangou Lv
Northwest Agriculture and Forestry University
Wen Zhao
Northwest Agriculture and Forestry University
Xinke Zhang
Northwest Agriculture and Forestry University
Yihua Zhang (zyh19620207@163.com)
https://orcid.org/0000-0002-6542-0976

Research article

Keywords: BMSC, sequencing, insulin producing cells, transdifferentiation, PPI, VIP, SSTR2, RPS6KA6

Posted Date: November 10th, 2020

DOI: https://doi.org/10.21203/rs.3.rs-32137/v2

Version of Record: A version of this preprint was published on February 25th, 2021. See the published version at https://doi.org/10.1186/s12864-021-07426-3.

Abstract

Background

Bone marrow mesenchymal stem cells are a potential resource for the clinical therapy of certain diseases. Canine, as a companion animal, living in the same space with human, is an ideal new model for human diseases research. Because of the high prevalence of diabetes, alternative transplantation islets resource (i.e. insulin producing cells) for diabetes treatment will be in urgent need, which makes our research on the transdifferentiation of Bone marrow mesenchymal stem cells into insulin producing cells become more important.

Result

In this study, we completed the transdifferentiation process and achieved the transcriptome profiling of five samples with two biological duplicates, namely, “BMSCs”, “islets”, “stage1”, “stage2” and “stage3”, and the latter three samples were achieved on the second, fifth and eighth day of induction. A total of 11,530 differentially expressed transcripts were revealed in the profiling data. The enrichment analysis of differentially expressed genes revealed several signaling pathways that are essential for regulating proliferation and transdifferentiation, including focal adhesion, ECM–receptor interaction, tight junction, protein digestion and absorption, and the Rap1 signaling pathway. Meanwhile, the obtained protein–protein interaction network and functional identification indicating involvement of three genes, *SSTR2*, *RPS6KA6*, and *VIP* could act as a foundation for further research.

Conclusion

In conclusion, to the best of our knowledge, this is the first survey of the transdifferentiation of canine BMSCs into insulin-producing cells according with the timeline using next-generation sequencing technology. The three key genes we pick out may regulate decisive genes during the development of transdifferentiation.

Background

Stem cells in particular for BMSCs have been used for decades for the treatment of many diseases. Numerous reports about the therapeutic potential of BMSCs have been published. BMSCs can be used for the regeneration of cartilage and osteochondral tissue defects [1], craniofacial tissue [2], and spinal cord [3]; moreover, type 1 diabetes can be treated using BMSC-derived insulin-producing cells [4]. The number of patients with diabetes is continuing to increase; according to the WHO (https://www.who.int/diabetes/global-report/en/), in 2016, 422 million individuals were affected by diabetes globally[5].

Pancreatic islet transplantation is available as an alternative therapy for diabetes, but it has the limitation of insufficient availability of islets; as such, many research teams have searched for other cells that could

substitute for islets. Human embryonic stem cell (hESC)- [6] and induced pluripotent stem cell (iPSC)-derived islet-like cells [7] have primarily been used to form islet-like clusters, but this is associated with a relatively high risk of neoplasia[8, 9] and other ethical issues[10]. Against this background, induced β cells derived from BMSCs are a promising option given that they are easy to obtain and immunoregulation[11, 12], and they can differentiate into osteoblasts, chondrocytes, and adipocytes[13, 14] in vitro. There are many ways to obtain insulin-producing cells using BMSCs. For example, it is possible to directly convert BMSCs into β-like cells by the lentiviral transduction of *NGN3*, *PDX1*, and *MAFA* [15]. Moreover, the addition of pancreas extract to the culture medium can be effective [16]. Another option is reprogramming, which can be achieved via the supplementation of small molecules such as conophylline [17].

Other groups reported that BMSC-derived vascular endothelial growth factor (VEGF) [18], epidermal growth factor (EGF) [19], and insulin-like growth factor 1 (IGF-1) [20] exhibited protective effects in many disease models and that the overexpression of several factors could indirectly mediate tissue repair [21]. The procedure for inducing pancreatic islet-like cells that we used in this study requires various factors, including pathway inhibitors and components EGF, bFGF, activin A, exendin-4, betacellulin, and nicotinamide[22-27], and it was a high efficient process compared with other research[26]. With this induction procedure, over 60 percentage human BMSCs turned into islet-like cell clusters[26, 27].

Different signaling pathways are involved when reprogramming occurs. For example, the AKT signaling pathway influences hypoxic stress and STZ stimulation [28], while ERK1/2 signaling pathway regulation confers resistance to apoptosis [29]. Many animal experiments have shown that co-transplantation of pancreatic islets and BMSCs can boost the survival rate of islets, which improves the efficiency of surgery [30]. Research has also demonstrated the essential role played by the extracellular matrix, directly interacting with cells, in determining the direction and fate of cell differentiation [31]. In summary, signaling pathways, the extracellular matrix, and transplantation methods can influence the rate of islet-like cell mass acquisition and the therapeutic efficiency of transplantation.

However, all of the available reprogramming methods are limited by the low efficiency of transformation [26, 32] [33, 34], which may lead to an insufficiency of pancreatic islets for transplantation surgery. This problem is associated with our limited understanding of the transdifferentiation mechanisms.

In this study, BMSCs were converted to islet-like cells by a three-step induction procedure and samples were collected at the end of each phase along with BMSCs and islets as negative and positive controls. Then, they were analyzed by transcriptome analysis, followed by enrichment analysis and PPI network analysis with three genes chosen for further research. The results obtained here could provide a foundation for future work to understand the mechanisms underlying the transdifferentiation of canine BMSCs into islet-like structures.

Results

Isolation and identification of BMSCs

When we transferred the mixture of cells extracted from bone marrow into dishes, we could only see the blood cells floating around, which is a necessary initial niche for the development of BMSCs. After 24 h of culture, the canine BMSCs presented an adherent state and fiber-like or irregular morphology; they also turned into spiral clusters when approaching confluence, which took approximately 6 days (Fig. 1A–C).

The results of flow cytometry assay confirmed that the BMSCs were positive for CD29, CD44, and CD166, and negative for CD11a, CD14, and CD34 (Fig. 1I).

To confirm the differentiation ability of BMSCs, we performed a three-lineage differentiation experiment; here, cell status was determined by staining tests, namely, Alizarin Red for osteoblasts (Fig. 1D), Alcian Blue for chondroblasts (Fig. 1E), and Oil Red O for adipocytes (Fig. 1F).

Induction and characterization of islet-like spheroids

At the nonadherent stage, BMSCs formed many spheroids floating in the medium (Fig. 1G). After the last induction stage, the spheroids were all positive for DTZ staining (Fig. 1H). The results of GSIS, 8.76 μIU/mL for DMEM low glucose (10mM) and 45.22 μIU/mL for DMEM high glucose (25mM) (Fig. 7K), confirmed that BMSCs had been transformed to pancreatic islet-like state.

De novo assembly

Pearson's correlation coefficients (R^2) were all around 0.9 for each biological replication of samples, which meant that these data were repeatable (Fig. 2B). The raw reads for each sample numbered around 100 million and the clean reads numbered about 90 million. Q20 and Q30 ranged from 96.67% to 97.12% and 91.87% to 92.76%, respectively, while the GC content ranged from 44.83% to 56.19% (Additional file 1). All clean reads, filtered by HISAT2, were used for comparison with the reference genome; in order for the reference genome to be considered suitable for this analysis and samples not to be contaminated, the rate of mapped reads should exceed 70%. The rate of total mapped reads was over 90% and the rates of uniquely mapped reads were all above 80% as prediction. (Additional file 2).

The quantitative analysis of common types of genes, such as miRNAs, tRNAs, and SRP-RNAs, using the software HTSeq, provided information on the status of different gene types based on the gene expression volume. The majority of genes were "protein-coding genes," representing 67.60% of the total on average.

Overview of DEGs

Based on the thresholds of $|\log2FC| > 1$ and $FDR < 0.05$, we subjected all types of transcripts to differential expression analysis. Differential transcript cluster analysis of mRNAs showed that there were 11,530 differentially expressed transcripts (Fig. 2A). The comparison of "BMSCs" and "stage1" showed that there were 555 upregulated genes and 569 downregulated ones (Fig. 2C), while there were 201 upregulated genes and 213 downregulated ones for the comparison between "stage 1" and "stage 2" (Fig. 2D), 232 and 132 for "stage 2" and "stage 3" (Fig. 2E), and 2,331 and 2,758 for "islets" vs "stage 3," respectively (Fig. 2F).

Enrichment analysis of DEGs from transcriptome sequencing and GEO data

All of the DEGs, including upregulated and downregulated transcripts, were annotated to signaling pathways related to the GO terms. For the KEGG pathway analysis, the “BMSCs vs. stage 1” DEGs were mapped to 230 KEGG pathways, while the “stage 1 vs. stage 2,” “stage 2 vs. stage 3,” and “islets vs. stage 3” DEGs were annotated to 163, 148, and 273 pathways, respectively. Considering RF and Q-value, we obtained the top 20 KEGG pathways for each comparison group, and they shared several of the same pathways, including tight junction, protein digestion and absorption, pancreatic secretion, focal adhesion, ECM–receptor interaction, Rap1 signaling pathway, and cell cycle (Fig. 3A–D). These pathways are significantly related to cell proliferation and differentiation, which control the fate of BMSCs when induce to differentiate.

The GO analysis of “BMSCs vs. stage 1” was dominated by CC and MF, which included the categories of nucleus, extracellular region, intracellular membrane-bound organelle, membrane-bound organelle; and protein binding, binding, ion binding, metal ion binding, cation binding, and transition metal ion binding (Fig. 4A). For “stage 1 vs. stage 2,” the DEGs were mainly annotated to the categories of cellular protein modification process, protein modification process, and phosphate-containing compound metabolic process for BP; cytoskeleton, non-membrane-bound organelle, and intracellular non-membrane-bound organelle for CC; and ion binding, cation binding, metal ion binding, binding, zinc ion binding, and ATP binding for MF (Fig. 4B). The comparison between “stage 2” and “stage 3” showed that binding activity still formed the majority of MF and that CC was still dominated by organelle; however, for BP, the main categories were the regulation of transcription, regulation of RNA biosynthetic process, and regulation of RNA metabolic process (Fig. 4C). Then, for the pair “islets vs. stage 3,” annotations included binding activities like those mentioned above for MF; additional extracellular region part, extracellular matrix, and mitochondrion for CC; and intracellular signal transduction, carbohydrate metabolic process, single-organism carbohydrate metabolic process, and small GTPase-mediated signal transduction for BP (Fig. 4D).

To further verify the results, we downloaded similar sample sources from GEO database for the comparison with our results. They were chosen from two datasets, GSE20113 and GSE52063, which belong to the same platform, GPL3738. We also chose three normal pancreas samples, namely, GSM502601, GSM502602, and GSM502603, from the first dataset, along with four BMSC samples, namely, GSM1258129, GSM1258130, GSM1258131, and GSM1258132, from the second dataset. Because of the different backgrounds of the samples, the normalization of these data was performed before enrichment analysis using R packages limma and gplots(Fig. 5A, B). There were 1,431 DEGs between those two series, 771 downregulated and 660 upregulated, showed in the heatmap (Fig. 5C). The top 20 KEGG pathways acquired from DAVID (Additional file 3), including focal adhesion, ECM–receptor interaction, and PI3K–Akt signaling pathway, represented the pathways with the highest enrichment scores. In terms of the GO results, chaperone-mediated protein folding and cellular zinc ion homeostasis for BP; and ion channel activity and oxidoreductase activity for MF (Additional file 4) are essential

processes of the pancreas. All these results are analogous to the findings of our samples from the transition of “BMSCs” to “islets.”

PPI network

The PPI network (Fig. 6) contained 1,406 nodes. Insulin, glucagon, and somatostatin represented key roles in this network based on the node size, so we analyzed the PPI network focusing on these three and those who linked to them by the first and second edges. Under these conditions, 168 nodes were shown in this network, and 22 nodes directly interacted with the three key genes.

Verification and quantification of key genes

The expression quantity of these 20 genes were verified by qRT-PCR, which was in accordance with the sequencing data (Fig. 7A). Among these genes, *SSTR2*, *RPS6KA6*, and *VIP* were picked out, transfected by lentivirus which were built for overexpression and knockdown of these three genes. It could be found that there were more spheroids in better shape than those who were knockdown (Fig. 7B-G). After the induction procedure, it was showed that the expression level of *PDX1*, *NGN3* and *NKX2.2* were upregulated in the overexpression groups of *VIP* and *RPS6KA6* (Fig. 7H, J), which was contrary for OE-*SSTR2* groups (Fig. 7I). The result gave us a hint that *VIP* and *RPS6KA6* might regulate the expression level of pancreas key genes *PDX1*, *NGN3* and *NKX2.2* through directly interaction or participating the signaling pathway such as MAPK signaling pathway in terms of *RPS6KA6* was a member of it. SSTR2, as a receptor of somatostatin, could have an effect on proliferation and differentiation via lowering cAMP [35]. Meanwhile, the GSIS (Fig. 7K) result was the same outcome.

Discussion

Canine BMSCs are advantageous source of pancreatic islet-like clusters

To the best of our knowledge, this is the first study analyzing the transdifferentiation of canine BMSCs according to the timeline of induction. Screening for DEGs between different timepoints was performed, and referring to pancreatic development, we could tell what state the cells were in during the induction, enabling adjustment of the induction procedure to achieve optimal conditions. The reason why we chose canine BMSCs for this study was as follow: (1) They can be easily derived from bone marrow, along with having another advantageous immune escape mechanism compared with other cell types such as ESCs and iPSCs[36-38]; (2) Another advantage is that the usage of and access to these latter two types of cell are often limited by ethical concerns[39]; (3) Canine has always been neglected to be a model animal with the increasing diabetes morbidity of companion dogs, and the same living environment with human can give more help for human diabetes treatment than mouse or any other animals [40, 41]; (4) Canine diabetes is more alike with human type I diabetes, but individual immune variation and environment can make big difference in the development of diabetes[42]. Some abnormal expressed genes involved with human diabetes have been identified in dog diabetes cases[43]. Based on the similar pathology and

physiology with human, canine without doubt is an ideal translational disease model for type I diabetes treatment in human[44].

For the first time induction procedure could be improved based on the transcriptome profiling data

At present, existing methods for induction have low efficiency [45], and no consensus has yet been reached regarding the mechanism of transdifferentiation of BMSCs into insulin producing cells. However, surprisingly, besides our team, no other groups have focused on the timeline-based analysis of the whole transition process of canine BMSCs, and with transcriptome profiling, the data has been uploaded on SRA database (https://www.ncbi.nlm.nih.gov/sra) with submission number SUB7457848.

The utility of GEO datasets is progressively expanding[46, 47]. In this research, several GEO-derived expression profiles obtained by array were considered. However, when limiting the selection to “canine species”, there were only 174 series selected from the database, which was too few for comparison with the total of 110,121 series of all GEO datasets (as of March 6, 2019). We screened out 71 series belonging to the same platform GPL3738, among which only three series had several samples related to the pancreas and BMSCs. Seven samples were chosen for the following data analysis as a reference and for verification of our profiling data. By using R package and online tool DAVID[48], these data were normalization and differentially expressed genes were extracted out to commit for enrichment analysis (Additional file 3,4).

Combined with the sequencing data, we found that all of the transcriptome profiling data and GEO data provided the same findings. The DEGs from each set of data were enriched in pathways such as those related to cell junction, PI3K–Akt signaling pathway, ECM–receptor interaction, Rap1 signaling pathway, cell cycle, and cell adhesion molecules (CAMs). The increased GO term binding activity including protein binding and ion binding reflected certain characteristics of the pancreas, generally related to vigorous secretory activity and calcium exchange [49]. Rap1 and Ras are all the downstream of ERK signaling as well as a part of MAPK signaling pathway[50], which can manipulate the transdifferentiation of BMSCs into IPCs by targeting FOS[51] to finally effect proliferation and differentiation of cells[52]. Cell junction and cell adhesion molecules can form a barrier with selection of small molecules, water and proteins to in and out cells to regulate cell differentiation[53, 54]. Under a nonadherent state during induction, cells exhibit similar protein expression pattern and intercellular junctions with organs in vivo[55], which means that cells could influence other cells via paracrine factors like EGF, VEGF, etc.[56].

PPI network analysis could screen out the genes among DEGs that are directly or indirectly regulated by each other, which could play an indispensable role in guiding future study of important regulatory factors in the process of induction. *VIP, SSTR2* and *RPS6KA6* were emerging from the network. After the overexpression and knockdown, we came to the conclusion that the two of them, *VIP* and *RPS6KA6*, had a positive effect on the induction of BMSCs to form islet-like clusters with relatively high insulin secretion, while the expression of *PDX1*, *NGN3* and *NKX2.2* had similar trend, which meant that these gene might interaction with each other. According to report, *VIP* can modulate BMSCs osteogenesis during bone repair[57], meanwhile, more research confirm that *VIP* can participate in immune activities by targeting

ILC3[58, 59]. Interestingly, *SSTR2* may involve in the rhythmic glucagon and insulin secretion[60]. However, there was little reference available about IPCs differentiation. Furthermore, these genes were participating in the same pathway like MAPK signaling pathway [61], Rap1 signaling pathway and Ras signaling pathway, and it could be a lead for the next-step mechanism research of the induction process to obtain high quality islet-like clusters.

Methods

Animals

The two Chinese rural dogs used in this experiment were purchased from the Experimental Animal Center of Northwest Agriculture and Forest University (Yangling, China). All animal experiments were carried out in accordance with our institute's laboratory animal requirements and the Guide for the Care and Use of Laboratory Animals (Ministry of Science and Technology of China, 2006).

Cultivation and identification of primary canine BMSCs

The BMSCs were extracted from the long bones of two female 3-month-old Chinese rural dogs, after anesthesia by injecting zoletil (0.1 ml/kg, Virbac Group, France). Followed by the experiment, they were committed to euthanasia with 200 mg/min intravenous infusion of propofol till no heartbeat. The bodies were collected by the Experimental Animal Center of Northwest Agriculture and Forest University (Yangling, China) for harmless disposal. For details about the separation of BMSCs, see our previous paper [62]. The cells were identified by flow cytometry and confirmed to undergo three-lineage differentiation the same as when proliferating in dishes [63]. Specifically, the potential for differentiating into the three lineages was assessed by a 7-day induction procedure. To induce osteogenic differentiation, a total of 2×10^4 cells were seeded into 12-well plates with α-MEM culture medium consisting of 10% FBS, 100 nmol/L dexamethasone, 30 μg/mL ascorbic acid, and 10 mmol/L β-glycerophosphate (Sigma-Aldrich, St. Louis, MO, USA). The medium for adipogenic differentiation contained 10% FBS, 1 μmol/L dexamethasone, 0.5 mmol/L isobutylmethylxanthine, 1 μg/mL insulin, and 100 μmol/L indomethacin (all from Sigma Aldrich). Chondrogenic differentiation medium was supplied with 10% FBS, 40 ng/mL dexamethasone, 50 μg/mL ascorbic acid, 50 μg/mL L-proline, 1 mmol/L sodium pyruvate (all from Sigma Aldrich), insulin–transferrin–selenium X (Gibco, Carlsbad, CA, USA), and 10 ng/mL transforming growth factor-β3 (PeproTech, Rocky Hill, NJ, USA), which was changed every 2 days.

The induction of BMSCs to transform into IPCs

The protocol used in this study involved three stages, while the BMSCs were placed in a suspended state to form spheroids, which mimicked the characteristics of islets in the pancreas. The dishes used in the protocol were all treated with 2-hydroxyethyl methacrylate (Sigma-Aldrich). In stage 1, passage 4 cells were cultured in Dulbecco's modified Eagle's medium (DMEM) high glucose (containing 17.5 mmol/L glucose; Hyclone, Logan, UT, USA), which contained 10 ng/ml basic fibroblast growth factor (bFGF; Invitrogen, Carlsbad, CA, USA), 10 ng/ml epidermal growth factor (EGF; Chemicon, CA, USA), 2% B27

supplement minus insulin (Gibco), 0.5% bovine serum albumin (BSA; Solarbio), and 0.1 mmol/L β-mercaptoethanol. Two days later, the medium was exchanged for stage 2 induction medium and supplied with DMEM high glucose with 10 ng/mL EGF, 20 ng/ml Activin A (Peprotech), 10 mmol/L nicotinamide (Sigma), 2% B27, 0.5% BSA, and 0.1 mmol/L β-mercaptoethanol for 3 days. Stage 3 also lasted 3 days, in which the spheroids were suspended in DMEM low glucose (containing 5.6 mmol/L glucose) with 10 ng/mL EGF, 10 nmol/L exendin-4 (Peprotech), 10 ng/mL betacellulin (Peprotech), 2% B27, 0.5% BSA, and 0.1 mmol/L β-mercaptoethanol. The medium was changed every 2 days.

Collecting those spheroids with a consistent size, we then performed DTZ staining as described previously and GSIS to determine whether a transition occurred after the induction procedure. The selected clusters were precultured in DMEM low glucose for 2 h to remove the insulin present, washed three times with PBS, and incubated in DMEM low glucose for 30 min. The supernatant was then collected and the clusters were transferred into DMEM high glucose stimulated for 30 min. The released insulin was tested by ELISA using Quantikine® ELISA kit, strictly in accordance with the operating instructions.

RNA extraction of cell clusters and quality control

Total RNA was extracted using TRIzol® reagent (Invitrogen, USA) following the manufacturer's protocol, and RNA degradation and contamination were monitored on 1% agarose gels, as well as the purity being checked using the NanoPhotometer® spectrophotometer (IMPLEN, CA, USA). RNA concentration was measured using Qubit® RNA Assay Kit in a Qubit® 2.0 Fluorometer (Life Technologies, CA, USA). Finally, RNA integrity, assessed by RIN8.0, was determined using the RNA Nano 6000 Assay Kit of the Bioanalyzer 2100 system (Agilent Technologies, CA, USA).

Library construction and sequencing processing

Ribosomal RNA was removed using the Epicentre Ribo-zero™ rRNA Removal Kit (Epicentre, USA), and an rRNA-free residue was obtained by ethanol precipitation. Subsequently, 3 μg of RNA per sample was used for library construction, which was generated using the rRNA-depleted RNA with the NEBNext® Ultra™ Directional RNA Library Prep Kit for Illumina® (NEB, USA), in accordance with the manufacturer's recommendations. To preferentially select cDNA fragments of 150–200 bp in length, the library fragments were purified with the AMPure XP system (Beckman Coulter, Beverly, USA). PCR was performed with Phusion High-Fidelity DNA polymerase, universal PCR primers, and Index (X) Primer. Finally, products were purified (AMPure XP system) and library quality was assessed on the Agilent Bioanalyzer 2100 system.

Cluster generation was performed on a cBot Cluster Generation System using TruSeq PE Cluster Kit v3-cBot-HS (Illumina), in accordance with the manufacturer's instructions. Subsequently, the sequencing data were processed on an Illumina Hiseq 4000 platform.

De novo assembly

Clean data were obtained after the processing of raw data through in-house Perl scripts. Q20, Q30, and GC content were calculated, with Q20 and Q30 representing the percentages of bases whose Phred [Phred=−10log10(e)] equaled or exceeded 20 and 30 relative to all bases. For mapping to the reference genome, the genome and gene model annotation files were downloaded directly from NCBI (https://www.ncbi.nlm.nih.gov/genome/?term=dog) and the annotation release ID was 105. The software HISAT2 v2.0.4[64] was used in this field. Finally, the mapped reads were assembled by StringTie (v1.3.1) [65] in a reference-based approach.

Identification of DEGs

FPKM was calculated based on the length of the fragments and count of reads mapped to this fragment. This was performed using cuffdiff (v2.1.1) and used to define the expression levels of coding genes. Transcripts with an adjusted P-value <0.05 were considered to be differentially expressed. As thresholds for defining significant differences in gene expression between samples, we used |log2FC| > 1 with a false discovery rate (FDR) < 0.05.

Enrichment analysis of DEGs and PPI analysis

Gene ontology (GO) was applied to annotate the functions of DEGs and lncRNAs, which were divided into three biological modules: molecular function (MF), cellular component (CC), and biological process (BP). This was implemented using the GOseq R package, with correction for bias in gene length [66]. GO terms with a corrected P-value less than 0.05 were considered to be significantly enriched with differentially expressed genes.

Kyoto Encyclopedia of Genes and Genomes (KEGG) pathway analysis was also adopted to define the functions of the DEGs and lncRNAs. We used KOBAS software to test the statistical significance of enrichment of differentially expressed genes and lncRNA target genes in KEGG pathways. The significance formula was the same as that in the GO analysis. The significance, which was calculated using the Q-value derived from multiple hypothesis testing of the P-value, was presented using the magnitude of −log10 (Q-value). Meanwhile, RF (rich factor) was defined as the ratio of DEGs relative to the overall annotated transcripts enriched in the same pathway.

PPI analysis of differentially expressed genes was based on the STRING database, which features known and predicted protein–protein interactions. Canine data were included in the database, so we constructed the networks by extracting the target gene list from the database. We visualized the findings using Cytoscape (v3.6.1).

Lentivirus vectors construction and transfection

The overexpression vector was pCDH-CMV-MCS-CopGFP-T2A-Puro, and complete coding sequences of target genes were synthesized by GeneCreat biological technology Co. (Wuhan, China). The vector used

for knockdown was CD513B-U6, and siRNAs were designed by BLOCK-iT™ RNAi Designer (https://rnaidesigner.thermofisher.com/rnaiexpress/). shRNAs derived from siRNAs were synthesized by TsingKe biological technology Co. (Beijing China).

qRT-PCR

Total RNA was extracted as described above, and cDNA was generated from total RNA. Primers for quantitative real time PCR (qRT-PCR) were designed using Primer Premier 5.0 software (Premier, Canada), and synthesized by TsingKe biological technology Co (Beijing China). qRT-PCR was performed on a Step One Plus™ Real-Time PCR System (Thermo Fisher Scientific, USA). Each 20 μL reaction mixture contained 10 μL of Maxima SYBR Green/ROX qPCR Master Mix (2X) (Thermo Scientific, USA), 0.3 μL of each primer (10 μM), 0.8 μL of cDNA, and 8.6 μL of nuclease-free water. The qRT-PCR run protocol was as follows: 95 °C, 10 min; followed by 40 cycles of 95 °C, 15 s; 60 °C, 30 s; and 72 °C, 15 s in 96-well optical reaction plates. Three biological replicates with three technical replicates for each value determined the Ct values. Expression levels of the tested reference genes were determined by Ct values and calculated by $2^{-\triangle\triangle Ct}$.

Bioinformatic analysis of data from the Gene Expression Omnibus (GEO) database using the DAVID database

The gene expression profiles GSE20113 nd GSE52063, chosen from GPL3738, were downloaded from the GEO database; these two series included three normal pancreas samples and four normal bone marrow mesenchymal stem cell samples derived from canine. Because these data were from the same platform, after normalization of the microarray data, we used R (https://www.r-project.org/) to acquire the DEGs, and analyzed these data using the DAVID database (https://david.ncifcrf.gov/).

Statistical analysis

SPSS 13.0 software was used for analysis of variance and paired T test. Measurement data were presented as mean ± SEM, $p < 0.05$ was statistically significant difference, expressed with (*); $0.01 < p < 0.05$ was expressed with (**); $p < 0.01$ for the extremely significant difference, expressed with (***); $p < 0.001$ was expressed with (****).

Conclusion

In this study, we have obtained an overview of the pathways involved in the regulation of BMSC transdifferentiation at different timepoints for the first time, and it makes a progress for learning the mechanism. Simultaneously, *VIP, SSTR2*, and *RPS6KA6* were selected out for their positive potential for the induction, and gain-and-lose function verification of them showed that *VIP,* and *RPS6KA6* could positively regulate *PDX1*, *NGN3* and *NKX2.2*, but *SSTR2* was on the contrary. We supposed that fine-tuning of these genes might contribute to transdifferentiation of BMSCs into IPCs and make an advance to the induction procedure.

Declarations

Ethics approval and consent to participate

The application named “The use of two Chinese rural dogs for the separation of BMSCs” were approved by the Animal Ethics Committee of Northwest Agriculture and Forest University (Animal Welfare Assurance no. NWAFU-AEC – 2018-11060076) at November 6, 2018. The consent to participate was permitted by the leader of institution Yihua Zhang.

Consent for publication

Not applicable.

Availability of data and material

Authors can confirm that all relevant data are included in the article and its supplementary information files, except for transcriptome data is uploaded on SRA with submission number: SUB7457848.

Author contributions

WJL and ZYH conceived the article, and WJL performed the experiments with data collection and analysis.

DPX, ZT, LYO, ZW and ZXK helped to collect and assemble data.

ZYH made the final approval of manuscript.

All authors have read and approved the manuscript.

Competing interests

The authors declare no conflict of interests/financial disclosure statement.

Funding

This work was supported by the National Natural Science Foundation of China (project number: 31872529) in the design of study, data collection, analysis .and writing of the manuscript.

Acknowledgments

We thank Novogene incorporated company at Beijing for their assistance in transcriptome analysis.

We thank Liwen Bianji, Edanz Group China (www.liwenbianji.cn/ac), for editing the English text of a draft of this manuscript.

Abbreviations

BMSCs	bone marrow mesenchymal stem cells
DEGs	differentially expressed genes
GSIS	glucose-stimulated insulin secretion
PPI	protein protein interaction
FPKM	fragments per kilobase of exon per million fragments mapped
IPCs	insulin producing cells
PDX1	pancreatic and duodenal homeobox 1
NGN3	neurogenin 3
NKX2.2	NK2 homeobox 2
VIP	Vasoactive Intestinal Peptide
SSTR2	Somatostatin Receptor 2
RPS6KA6	Ribosomal Protein S6 Kinase A6
BP	biological process
MF	molecular function
CC	cell component

References

1. Francesca V, Gianluca G, Matilde T, Veronica B, Nicolò NA, Milena F: **Clinical use of bone marrow, bone marrow concentrate, and expanded bone marrow mesenchymal stem cells in cartilage disease**. *Stem Cells & Development* 2013, **22**(2):181.
2. Yang M, Zhang H, Gangolli R: **Advances of mesenchymal stem cells derived from bone marrow and dental tissue in craniofacial tissue engineering**. *Current stem cell research & therapy* 2014, **9**(3):150-161.
3. Lin L, Lin H, Bai S, Zheng L, Zhang X: **Bone marrow mesenchymal stem cells (BMSCs) improved functional recovery of spinal cord injury partly by promoting axonal regeneration**. *Neurochemistry International* 2018:S0197018617305703.
4. Godfrey KJ, Mathew B, ., Bulman JC, Shah O, ., Clement S, ., Gallicano GI: **Stem cell-based treatments for Type 1 diabetes mellitus: bone marrow, embryonic, hepatic, pancreatic and induced pluripotent stem cells**. *Diabetic Medicine A Journal of the British Diabetic Association* 2011, **29**(1):14-23.

5. **global report on diabetes** [https://www.who.int/diabetes/global-report/en/]
6. Thomson JA, Itskovitz-Eldor J, ., Shapiro SS, Waknitz MA, Swiergiel JJ, Marshall VS, Jones JM: **Embryonic stem cell lines derived from human blastocysts**. *Science* 1998.
7. Ianus A, Holz GG, Theise ND, Hussain MA: **In vivo derivation of glucose-competent pancreatic endocrine cells from bone marrow without evidence of cell fusion**. *J Clin Invest* 2003, **111**(6):843-850.
8. Abad M, Mosteiro L, Pantoja C, Cañamero M, Rayon T, Ors I, Graña O, Megías D, Domínguez O, Martínez D *et al*: **Reprogramming in vivo produces teratomas and iPS cells with totipotency features**. *Nature* 2013, **502**(7471):340-345.
9. Zhao X-y, Li W, Lv Z, Liu L, Tong M, Hai T, Hao J, Guo C-l, Ma Q-w, Wang L *et al*: **iPS cells produce viable mice through tetraploid complementation**. *Nature* 2009, **461**(7260):86-90.
10. Ding D-C, Shyu W-C, Lin S-Z: **Mesenchymal stem cells**. *Cell Transplant* 2011, **20**(1).
11. Shahjalal HM, Abdal Dayem A, Lim KM, Jeon T-l, Cho S-G: **Generation of pancreatic β cells for treatment of diabetes: advances and challenges**. *Stem cell research & therapy* 2018, **9**(1):355.
12. Päth G, Perakakis N, Mantzoros CS, Seufert J: **Stem cells in the treatment of diabetes mellitus - Focus on mesenchymal stem cells**. *Metabolism* 2019, **90**.
13. Pan K, Sun Q, Zhang J, Ge S, Li S, Zhao Y, Yang P: **Multilineage differentiation of dental follicle cells and the roles of Runx2 over-expression in enhancing osteoblast/cementoblast-related gene expression in dental follicle cells**. *Cell Prolif* 2010, **43**(3):219-228.
14. Elsafadi M, Manikandan M, Atteya M, Hashmi JA, Iqbal Z, Aldahmash A, Alfayez M, Kassem M, Mahmood A: **Characterization of Cellular and Molecular Heterogeneity of Bone Marrow Stromal Cells**. *Stem Cells Int* 2016, **2016**:9378081.
15. Zhou Q, Brown J, Kanarek A, Rajagopal J, Melton DA: **In vivo reprogramming of adult pancreatic exocrine cells to beta-cells**. *Nature* 2008, **455**(7213):627-632.
16. Kyung Suk C, Jun-Seop S, Jae-Jeong L, Young Soo K, Seung-Bum K, Chan-Wha K: **In vitro trans-differentiation of rat mesenchymal cells into insulin-producing cells by rat pancreatic extract**. *Biochemical & Biophysical Research Communications* 2005, **330**(4):1299-1305.
17. Hisanaga E, Park K, Yamada S, H, Takeuchi T, Mori M, Seno M, Umezawa K, Takei I, Kojima I: **A simple method to induce differentiation of murine bone marrow mesenchymal cells to insulin-producing cells using conophylline and betacellulin-delta4**. *Endocrine Journal* 2008, **55**(3):535-543.
18. Eckhard L, Guqiang G, Margaret ML, Dennis B, Rolf B, Lewis Charles M, Hans Peter G, Napoleone F, Melton DA: **Role of VEGF-A in vascularization of pancreatic islets**. *Current Biology* 2003, **13**(12):1070-1074.
19. Lemper M, Groef SD, Stangé G, Baeyens L, Heimberg H: **A combination of cytokines EGF and CNTF protects the functional beta cell mass in mice with short-term hyperglycaemia**. *Diabetologia* 2016, **59**(9):1-11.

20. Sakaguchi M, Fujisaka S, Cai W, Winnay JN, Konishi M, O'Neill BT, Li M, Takahashi H, Hu J: **Adipocyte Dynamics and Reversible Metabolic Syndrome in Mice with an Inducible Adipocyte-Specific Deletion of the Insulin Receptor**. *Cell Metabolism* 2017, **25**(2):448.
21. Ryang Hwa L, Joo Youn O, Hosoon C, Nikolay B: **Therapeutic factors secreted by mesenchymal stromal cells and tissue repair**. *Journal of Cellular Biochemistry* 2011, **112**(11):3073-3078.
22. Zhang D, Jiang W, Liu M, Sui X, Yin X, Chen S, Shi Y, Deng H: **Highly efficient differentiation of human ES cells and iPS cells into mature pancreatic insulin-producing cells**. *Cell Res* 2009, **19**(4):429-438.
23. Russ HA, Parent AV, Ringler JJ, Hennings TG, Nair GG, Shveygert M, Guo T, Puri S, Haataja L, Cirulli V *et al*: **Controlled induction of human pancreatic progenitors produces functional beta-like cells in vitro**. *EMBO J* 2015, **34**(13):1759-1772.
24. Segev H, Fishman B, Ziskind A, Shulman M, Itskovitz-Eldor J: **Differentiation of human embryonic stem cells into insulin-producing clusters**. *Stem cells (Dayton, Ohio)* 2004, **22**(3):265-274.
25. Kim H-S, Hong S-H, Oh S-H, Kim J-H, Lee M-S, Lee M-K: **Activin A, exendin-4, and glucose stimulate differentiation of human pancreatic ductal cells**. *J Endocrinol* 2013, **217**(3):241-252.
26. Zhang Y, Dou Z: **Under a nonadherent state, bone marrow mesenchymal stem cells can be efficiently induced into functional islet-like cell clusters to normalize hyperglycemia in mice: a control study**. *Stem Cell Research & Therapy* 2014, **5**(3):66.
27. Zhang YH, Dou ZY, Shen WZ, Yang CR, Gao ZM: **Isolation and Culture of Bone Marrow Mesenchymal Stem Cells from Human Fetus and Its Biological Properties**. *Journal of Agricultural Biotechnology* 2008, **5**(3):237-244.
28. Liang X, Ding Y, Lin F, Zhang Y, Zhou X, Meng Q, Lu X, Jiang G, Zhu H, Chen Y *et al*: **Overexpression of ERBB4 rejuvenates aged mesenchymal stem cells and enhances angiogenesis via PI3K/AKT and MAPK/ERK pathways**. *FASEB journal : official publication of the Federation of American Societies for Experimental Biology* 2019, **33**(3):4559-4570.
29. Liu C, Zhang W, Peradze N, Lang L, Straetener J, Feilen PJ, Alt M, Jäger C, Laubner K, Perakakis N: **Mesenchymal stem cell (MSC)-mediated survival of insulin producing pancreatic β-cells during cellular stress involves signalling via Akt and ERK1/2**. *Molecular & Cellular Endocrinology* 2018, **473**:S0303720718300479.
30. He Y, Zhang D, Zeng Y, Ma J, Wang J, Guo H, Zhang J, Wang M, Zhang W, Gong N: **Bone Marrow-Derived Mesenchymal Stem Cells Protect Islet Grafts Against Endoplasmic Reticulum Stress-Induced Apoptosis During the Early Stage After Transplantation**. *Stem cells* 2018, **36**(7):1045-1061.
31. Mamidi A, Prawiro C, Seymour PA, de Lichtenberg KH, Jackson A, Serup P, Semb H: **Mechanosignalling via integrins directs fate decisions of pancreatic progenitors**. *Nature* 2018, **564**(7734):114-118.
32. Czubak P, Bojarska-Junak A, Tabarkiewicz J, Putowski L: **A modified method of insulin producing cells' generation from bone marrow-derived mesenchymal stem cells**. *Journal of Diabetes Research* 2014, **2014**(1):628591.

33. Katuchova J, Harvanova D, Spakova T, Kalanin R, Farkas D, Durny P, Rosocha J, Radonak J, Petrovic D, Siniscalco D: **Mesenchymal Stem Cells in the Treatment of Type 1 Diabetes Mellitus**. *Endocrine Pathology* 2015, **26**(2):95-103.
34. Dave SD, P CN, P JV, T UG: **In Vitro Generated Mesenchymal Stem Cells: Suitable Tools To Target Insulin Dependent Diabetes Mellitus?***Current Stem Cell Research & Therapy* 2016, **12**(4).
35. Elliott AD, Ustione A, Piston DW: **Somatostatin and insulin mediate glucose-inhibited glucagon secretion in the pancreatic α-cell by lowering cAMP**. *Am J Physiol Endocrinol Metab* 2015, **308**(2):E130-E143.
36. Yang Z, He C, He J, Chu J, Liu H, Deng X: **Curcumin-mediated bone marrow mesenchymal stem cell sheets create a favorable immune microenvironment for adult full-thickness cutaneous wound healing**. *Stem cell research & therapy* 2018, **9**(1):21.
37. Liu S, Stroncek DF, Zhao Y, Chen V, Shi R, Chen J, Ren J, Liu H, Bae HJ, Highfill SL *et al*: **Single cell sequencing reveals gene expression signatures associated with bone marrow stromal cell subpopulations and time in culture**. *J Transl Med* 2019, **17**(1):23.
38. Abbuehl J-P, Tatarova Z, Held W, Huelsken J: **Long-Term Engraftment of Primary Bone Marrow Stromal Cells Repairs Niche Damage and Improves Hematopoietic Stem Cell Transplantation**. *Cell Stem Cell* 2017, **21**(2).
39. Breithardt G: **The ESC Ethics Committee**. *Eur Heart J* 2019, **40**(28):2284-2286.
40. Adin CA, Gilor C: **The Diabetic Dog as a Translational Model for Human Islet Transplantation**. *Yale J Biol Med* 2017, **90**(3):509-515.
41. Catchpole B, Ristic JM, Fleeman LM, Davison LJ: **Canine diabetes mellitus: can old dogs teach us new tricks?***Diabetologia* 2005, **48**(10):1948-1956.
42. Nelson RW, Reusch CE: **Animal models of disease: classification and etiology of diabetes in dogs and cats**. *J Endocrinol* 2014, **222**(3):T1-T9.
43. Catchpole B, Adams JP, Holder AL, Short AD, Ollier WER, Kennedy LJ: **Genetics of canine diabetes mellitus: are the diabetes susceptibility genes identified in humans involved in breed susceptibility to diabetes mellitus in dogs?***Vet J* 2013, **195**(2):139-147.
44. Moshref M, Tangey B, Gilor C, Papas KK, Williamson P, Loomba-Albrecht L, Sheehy P, Kol A: **Concise Review: Canine Diabetes Mellitus as a Translational Model for Innovative Regenerative Medicine Approaches**. *Stem Cells Transl Med* 2019, **8**(5):450-455.
45. Orive G, Emerich D, Khademhosseini A, Matsumoto S, Hernández RM, Pedraz JL, Desai T, Calafiore R, Vos PD: **Engineering a Clinically Translatable Bioartificial Pancreas to Treat Type I Diabetes**. *Trends in Biotechnology* 2018, **36**(4):S0167779918300283.
46. Toro-Domínguez D, Martorell-Marugán J, López-Domínguez R, García-Moreno A, González-Rumayor V, Alarcón-Riquelme ME, Carmona-Sáez P: **ImaGEO: integrative gene expression meta-analysis from GEO database**. *Bioinformatics* 2019, **35**(5):880-882.
47. Wang J, Wang Y, Kong F, Han R, Song W, Chen D, Bu L, Wang S, Yue J, Ma L: **Identification of a six-gene prognostic signature for oral squamous cell carcinoma**. *J Cell Physiol* 2020, **235**(3):3056-3068.

48. Huang DW, Sherman BT, Lempicki RA: **Systematic and integrative analysis of large gene lists using DAVID bioinformatics resources**. *Nature protocols* 2009, **4**(1):44-57.
49. Cano DA, Matthias H, Martin Z: **Pancreatic development and disease**. *Gastroenterology* 2007, **132**(2):745-762.
50. Shah S, Brock EJ, Ji K, Mattingly RR: **Ras and Rap1: A tale of two GTPases**. *Semin Cancer Biol* 2019, **54**:29-39.
51. Wu D-M, Zhang Y-T, Lu J, Zheng Y-L: **Effects of microRNA-129 and its target gene c-Fos on proliferation and apoptosis of hippocampal neurons in rats with epilepsy via the MAPK signaling pathway**. *J Cell Physiol* 2018, **233**(9):6632-6643.
52. Ohguchi H, Harada T, Sagawa M, Kikuchi S, Tai YT, Richardson PG, Hideshima T, Anderson KC: **KDM6B modulates MAPK pathway mediating multiple myeloma cell growth and survival**. *Leukemia* 2017, **31**(12):2661-2669.
53. Díaz-Coránguez M, Liu X, Antonetti DA: **Tight Junctions in Cell Proliferation**. *Int J Mol Sci* 2019, **20**(23).
54. Wiesner M, Berberich O, Hoefner C, Blunk T, Bauer-Kreisel P: **Gap junctional intercellular communication in adipose-derived stromal/stem cells is cell density-dependent and positively impacts adipogenic differentiation**. *J Cell Physiol* 2018, **233**(4):3315-3329.
55. Abbott A: **Cell culture: biology's new dimension**. *Nature* 2003, **424**(6951):870-872.
56. Butt H, Mehmood A, Ali M, Tasneem S, Tarar MN, Riazuddin S: **Vitamin E preconditioning alleviates in vitro thermal stress in cultured human epidermal keratinocytes**. *Life Sci* 2019, **239**:116972.
57. Shi L, Feng L, Zhu M-L, Yang Z-M, Wu T-Y, Xu J, Liu Y, Lin W-P, Lo JHT, Zhang J-F *et al*: **Vasoactive Intestinal Peptide Stimulates Bone Marrow-Mesenchymal Stem Cells Osteogenesis Differentiation by Activating Wnt/β-Catenin Signaling Pathway and Promotes Rat Skull Defect Repair**. *Stem Cells Dev* 2020, **29**(10):655-666.
58. Seillet C, Luong K, Tellier J, Jacquelot N, Shen RD, Hickey P, Wimmer VC, Whitehead L, Rogers K, Smyth GK *et al*: **The neuropeptide VIP confers anticipatory mucosal immunity by regulating ILC3 activity**. *Nat Immunol* 2020, **21**(2):168-177.
59. Talbot J, Hahn P, Kroehling L, Nguyen H, Li D, Littman DR: **Feeding-dependent VIP neuron-ILC3 circuit regulates the intestinal barrier**. *Nature* 2020, **579**(7800):575-580.
60. Petrenko V, Dibner C: **Cell-specific resetting of mouse islet cellular clocks by glucagon, glucagon-like peptide 1 and somatostatin**. *Acta Physiol (Oxf)* 2018, **222**(4):e13021.
61. Rafiee M, Keramati MR, Ayatollahi H, Sadeghian MH, Barzegar M, Asgharzadeh A, Alinejad M: **Down-Regulation of Ribosomal S6 kinase RPS6KA6 in Acute Myeloid Leukemia Patients**. *Cell journal* 2016, **18**(2):159-164.
62. Chen C, Zheng S, Zhang X, Dai P, Gao Y, Nan L, Zhang Y: **Transplantation of amniotic scaffold seeded mesenchymal stem cells and/or endothelial progenitor cells from bone marrow to efficiently repair 3-cm circumferential urethral defect in model dogs**. *Tissue Engineering Part A* 2017:ten.TEA.2016.0518.

63. Dominici M, ., Blanc K, Le, Mueller I, ., Slaper-Cortenbach I, ., Fc M, Rj D, Keating A, ., Dj P, Em H: **Minimal criteria for defining multipotent mesenchymal stromal cells. The International Society for Cellular Therapy position statement**. *Cytotherapy* 2006.
64. Daehwan K, Ben L, Salzberg SL: **HISAT: a fast spliced aligner with low memory requirements**. *Nature Methods* 2015, **12**(4):357-360.
65. Pertea M, Kim D, Pertea GM, Leek JT, Salzberg SL: **Transcript-level expression analysis of RNA-seq experiments with HISAT, StringTie and Ballgown**. *Nature Protocols* 2016, **11**(9):1650.
66. Young MD, Wakefield MJ, Smyth GK, Oshlack A: **Gene ontology analysis for RNA-seq: accounting for selection bias**. *Genome Biology* 2010, **11**(2):R14-R14.

Additional Files

Additional file 1. xlsx -A summary of the quality of output data. “Clean bases” — The number of reads multiplied by the length of the sequence is converted to G. “Error rate” — Error rate of base sequencing. “Q20” and “Q30” represented the percentage of bases with Phred value greater than 20 and 30 in the total base. “GC content” represented the percentage of total bases G and C.

Additional file 2. xlsx - A comparison of mapped reads and the reference genome alignment. “Total mapped” — The number of reads that can be mapped to the genome. “Uniquely mapped” — The number of reads with a unique matched alignment position on the reference sequence. “Multiple mapped” — The number of reads with multipul matched alignment positions on the reference sequence. “Reads map to '+'” — The reads that can map to the sense strand of genome. “Reads map to '-'” — The reads that can map to the antisense strand of genome. “Non-splice reads” — The number of the intact Uniquely mapped reads which map to exons. “Splice reads” — The number of the segmented Uniquely mapped reads which map to exons. Our samples owned relatively high quality with over 90% mapped clean reads.

Additional file 3.xlsx - KEGG analysis of GEO data using DAVID. It was top 20 signaling pathways showed in this table. “Enrichment Score” — The overall enrichment score for each term members, the higher, the more enriched. “Count” — The number of genes involved in individual term. “Banjamini” — The modified Fisher Exact P-Value, the smaller, the more enriched.

Additional file 4. xlsx - Top 20 items of GO analysis of GEO data. “Enrichment Score” — The overall enrichment score for each term members, the higher, the more enriched. “Count” — The number of genes involved in individual term. “Banjamini” — The modified Fisher Exact P-Value, the smaller, the more enriched.

Figures

FIGURE 1

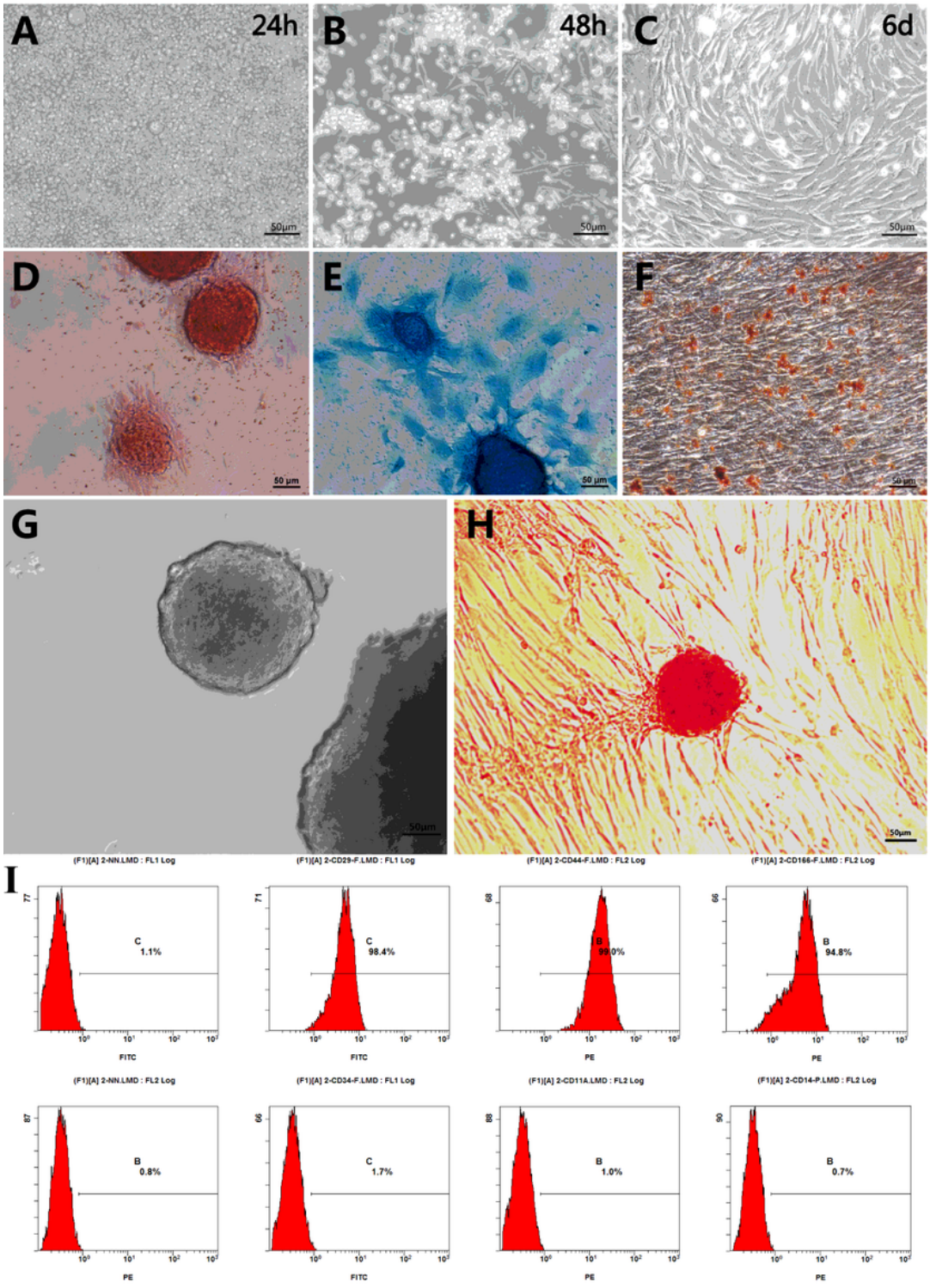

Figure 1

The separation, identification and induction of BMSCs. A 24 hours after the separation, only blood cells could be seen in the dish. B Two days later, with replacement of medium several attached BMSCs, which were in spindle shape, could be seen. C When it came to 6 days, the BMSCs grew vortically. D This was the alizarin red staining for the osteoblasts, which meant that BMSCs could different into osteoblasts. E The differentiation of BMSCs to chondroblasts was confirmed by alcian blue staining. F BMSCs were

positive for the oil red O staining when BMSCs were induced to adipocytes. G The induction procedure was performed under a nonadherent state and the spheroids were ranged from 100 to 200 μm. H After the last step of induction, the reattached clusters were stained by DTZ, and they showed brownish red. (scale bar = 50 μm). I The flow cytometry of BMSCs.

FIGURE 2

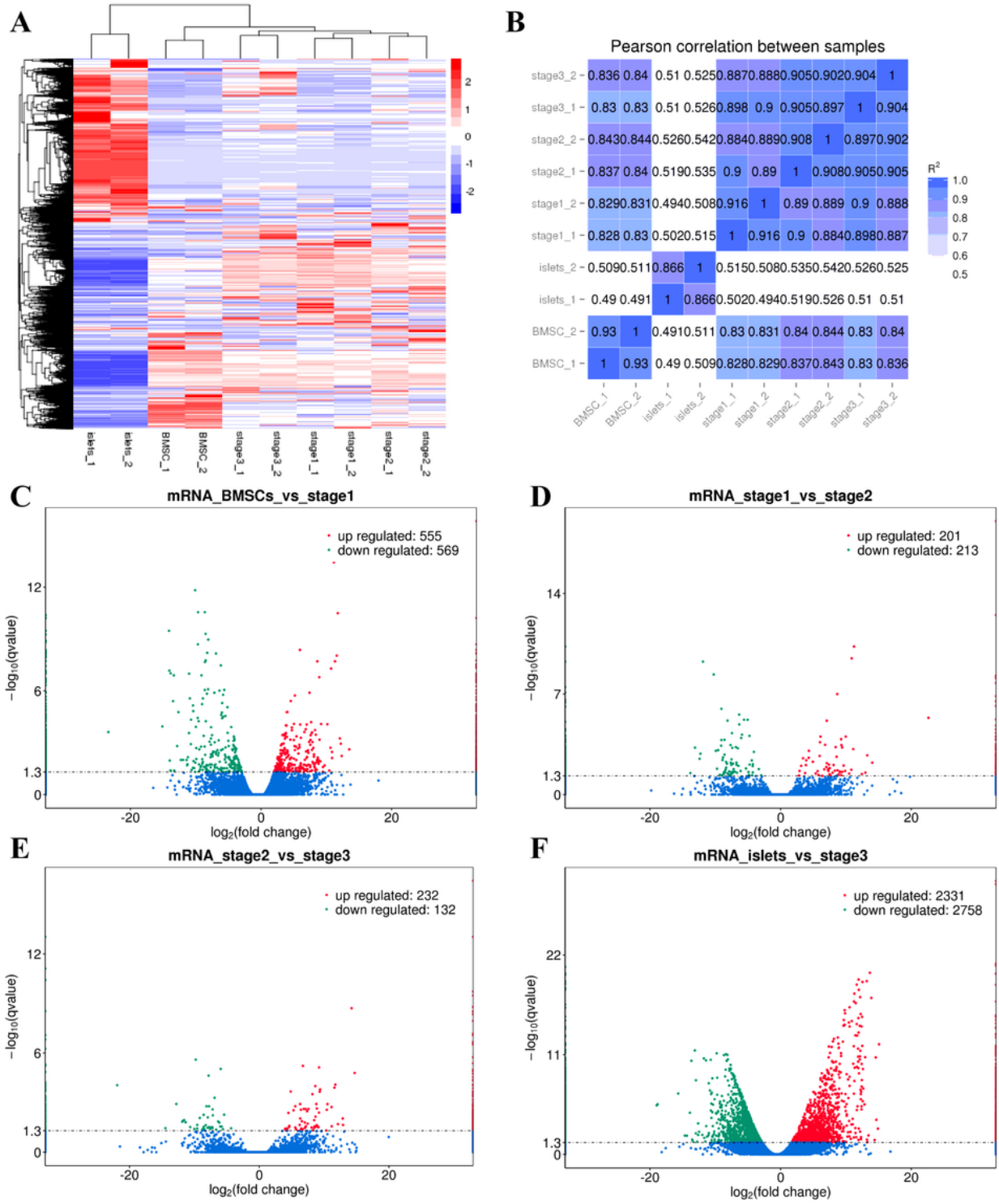

Figure 2

DEGs of different groups. A Heatmap illustrated differentially expressed genes of known transcripts which were screened based on |log2FC| > 1 and FDR < 0.05. B The person correlation coefficients of every two samples and the repeatability of these samples were confirmed, meanwhile, the variation of different samples could also be seen. C-F The volcano maps for up regulated and down regulated genes between different samples “BMSCs vs stage1”, “stage1 vs stage2”, “stage2 vs stage3” and “islets vs stage3”.

FIGURE 3

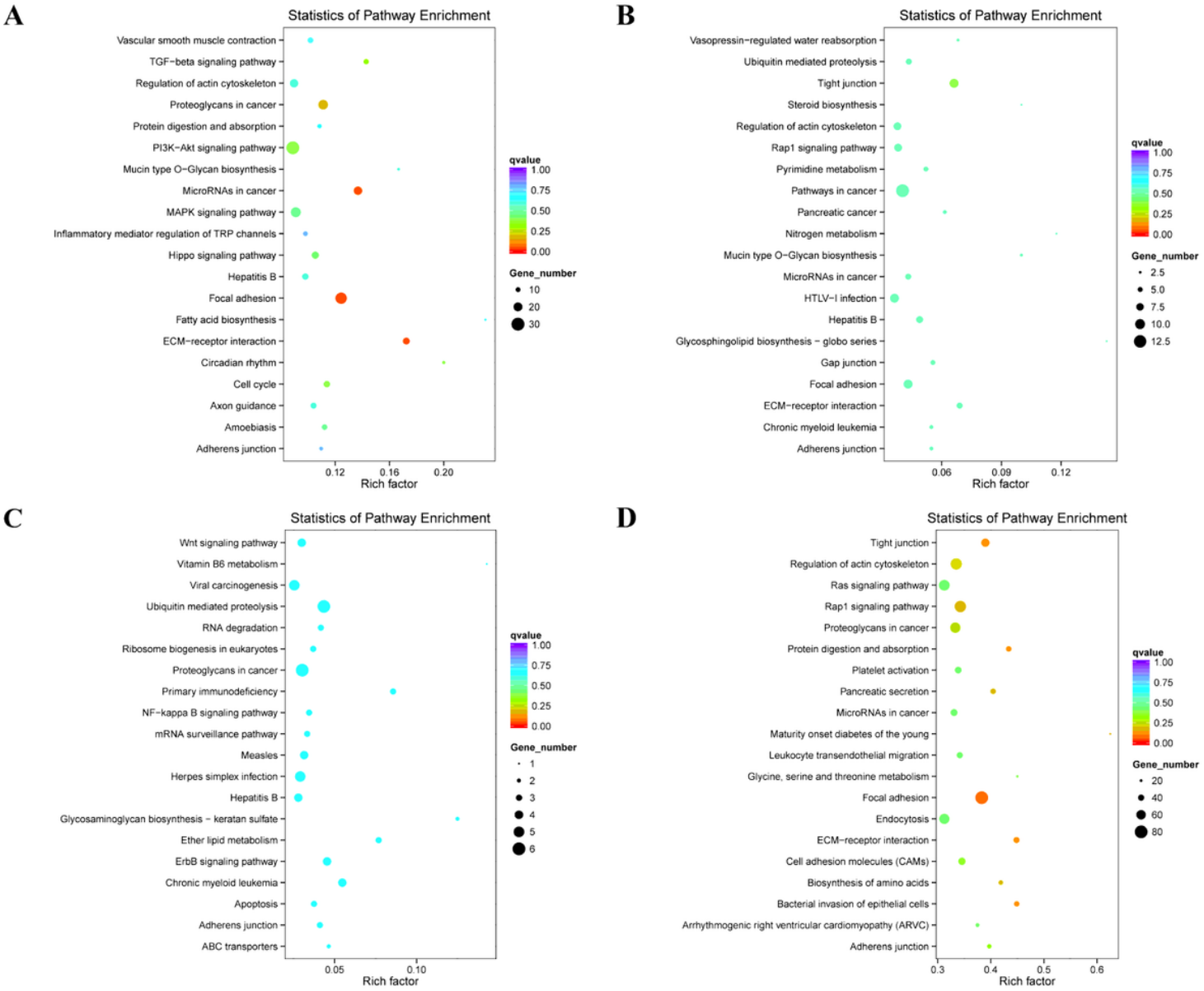

Figure 3

Top 20 KEGG signaling pathways of known transcripts, the size of bubbles represented for mapped gene numbers of the item, and the color was measured by the Qvalue. A KEGG analysis of DEGs of “BMSCs vs islets” showed that focal adhesion, protein digestion and absorption and tight junction were the dominant signals. B KEGG analysis of DEGs of “BMSCs vs stage3” showed that focal adhesion, ECM-receptor interaction and cell cycle were the main pathways. C KEGG analysis of “islets vs stage3” showed that

focal adhesion, ECM-receptor interaction and tight junction were the most part, which almost the same as the former two results.

FIGURE 4

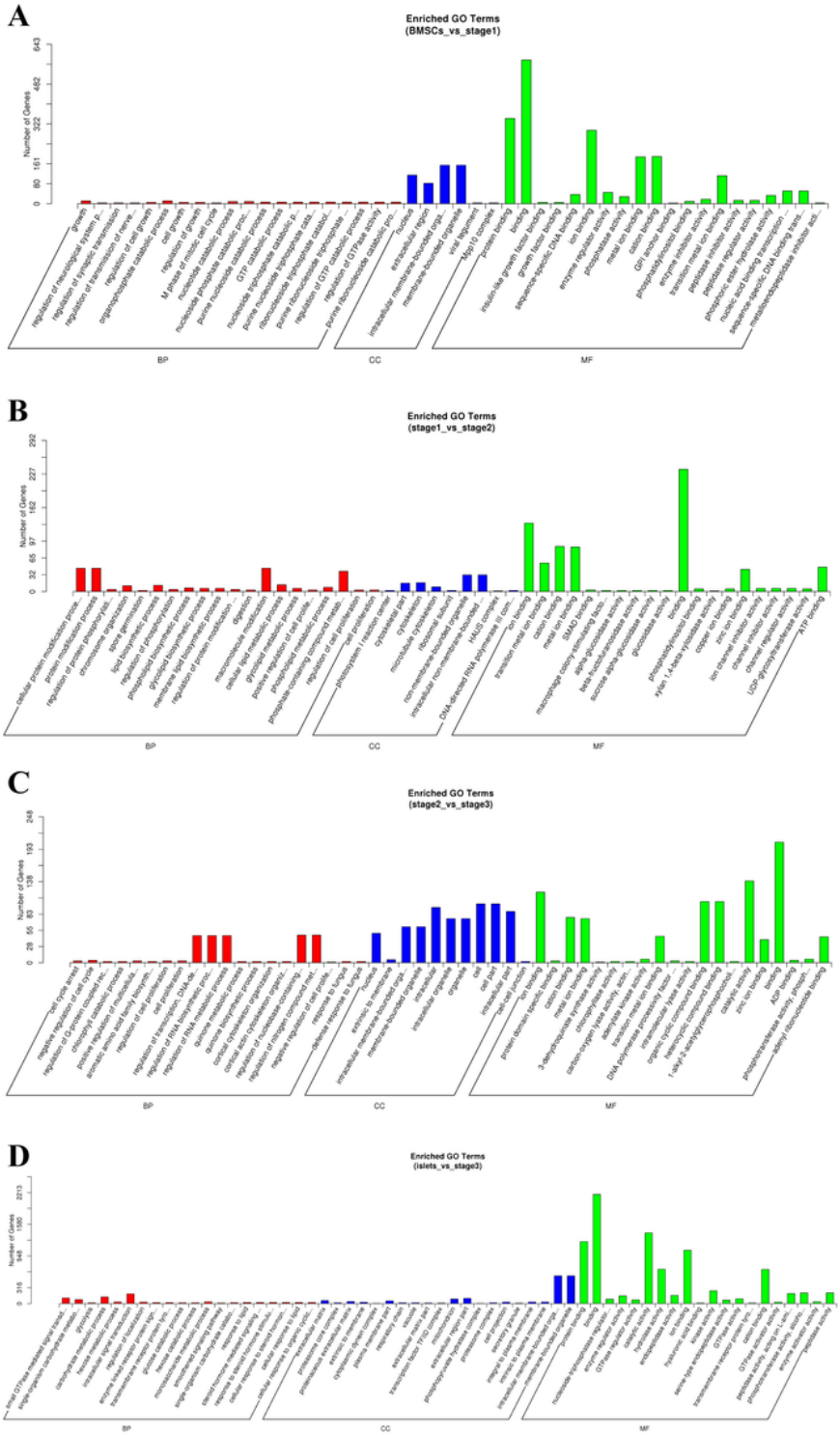

Figure 4

Top 20 GO items demonstrated that the MF and CC usually are the dominate part of GO. A GO analysis for “BMSCs vs stage1”. B GO analysis for “stage1 vs stage2”. C GO analysis for “stage2 vs stage3”, D GO analysis for “islets vs stage3”

FIGURE 5

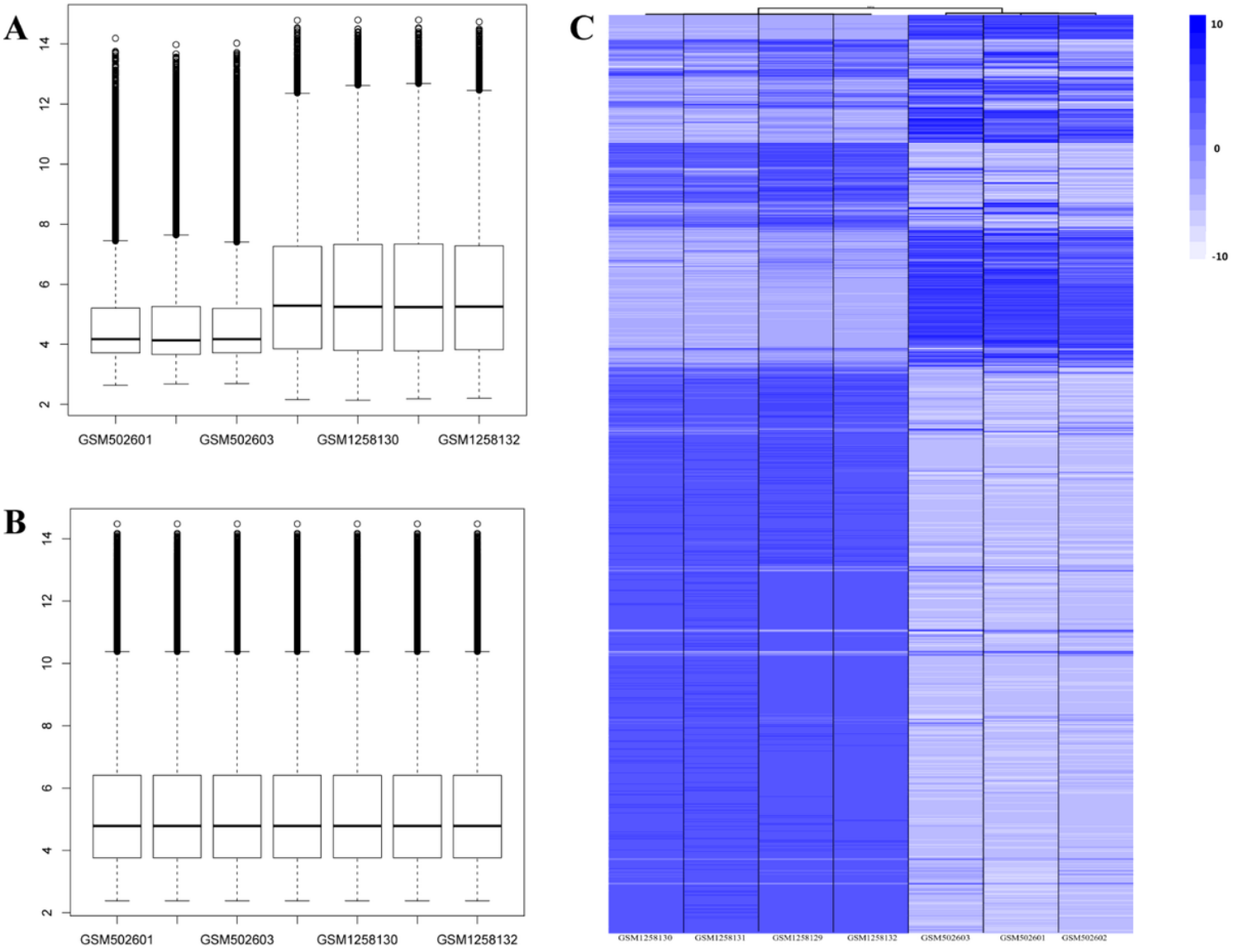

Figure 5

Normalization and enrichment analysis of GEO data. A The status of the raw data from GEO database showed in box-plot. B Normalized data showed in box-plot, and the median was at the same level. C DEGs of GEO data, the expression level low to high were showed by light to dark blue.

FIGURE 6

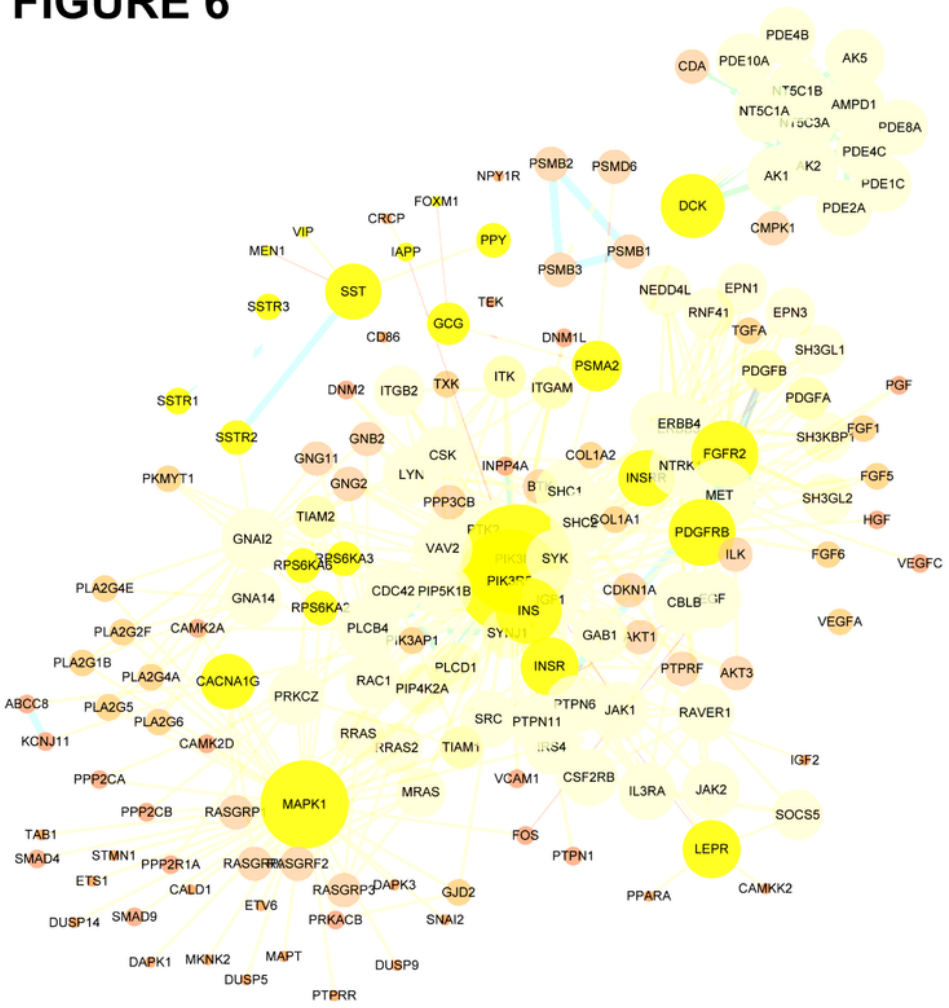

Figure 6

PPI network analysis of known transcripts. The size and color of nodes meant the number of genes related and betweenness centrality, the color and width of edges meant the PPI score of each two genes.

FIGURE 7

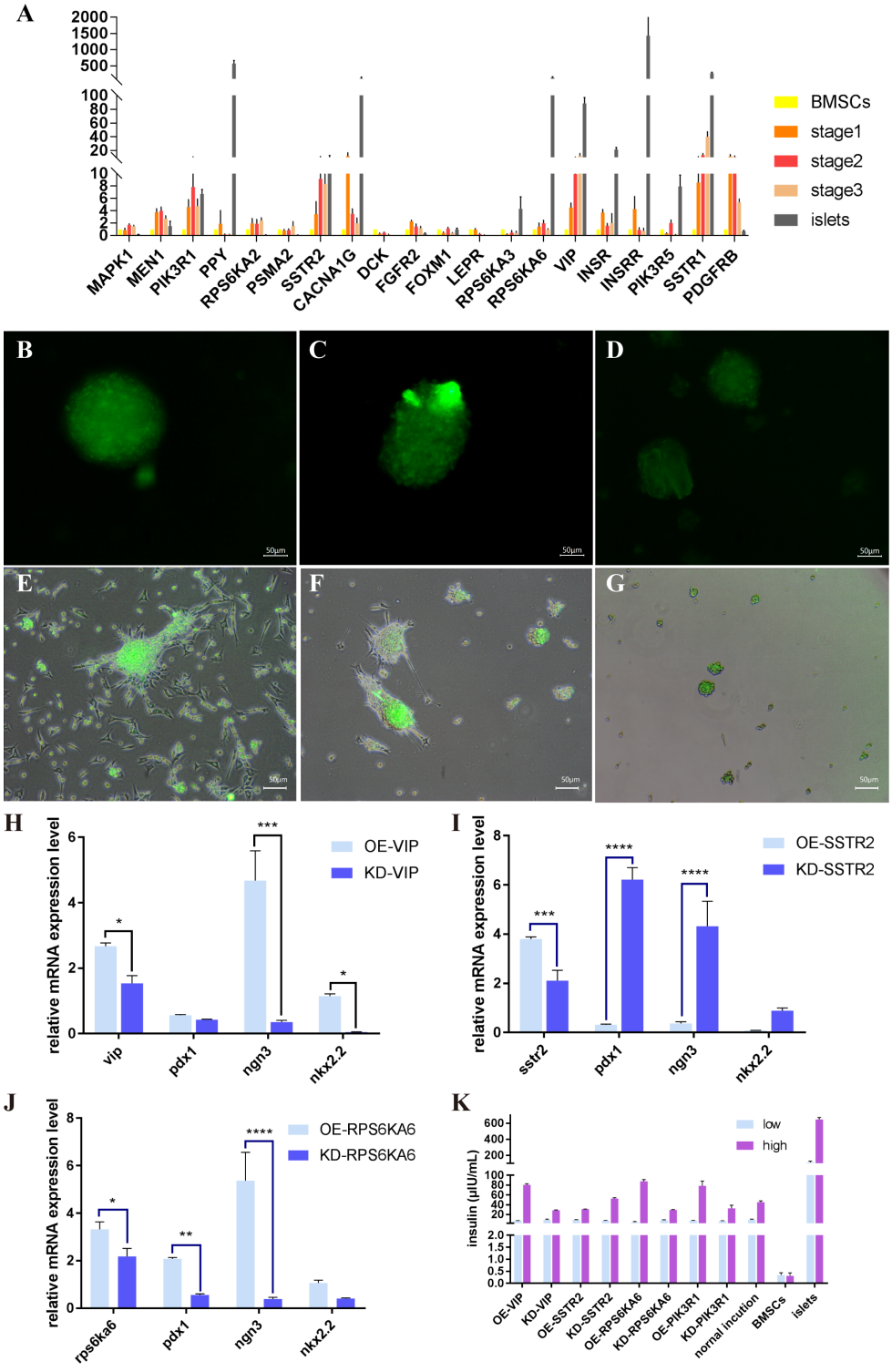

Figure 7

A The verification of the 20 key genes by qRT-PCR. B-D Overexpression of VIP, SSTR2 and RPS6KA6 respectively, 48h after transfection. E-G Knockdown of VIP, SSTR2 and RPS6KA6, the bright fields were merged with fluorescence images. (scale bar = 50 μm) H qRT-PCR of OE-VIP and KD-VIP after induction, “*”means 0.01 < p value <0.05, “**” 0.001< means p value <0.01, “***” means 0.0001 < p value <0.001, “****” means p value < 0.0001. I qRT-PCR of OE-SSTR2 and KD-SSTR2 after induction. J qRT-PCR of OE-

RPS6KA6 and KD-RPS6KA6 after induction. K The GSIS results of overexpression and knockdown of VIP, SSTR2 and RPS6KA6 and normal induction groups are control samples.

Supplementary Files

This is a list of supplementary files associated with this preprint. Click to download.

- Additionalfile4.xlsx
- Additionalfile3.xlsx
- Additionalfile2.xlsx
- Additionalfile1.xlsx